

AD-A191 164

COORDINATED GROUND AND SPACE MEASUREMENTS OF AURORAL
SURGE OVER SOUTH POL. (U) AEROSPACE CORP ET SEGUNDO CA
SPACE SCIENCES LAB 1 J ROSENBERG ET AL. 81 174 88

1/1

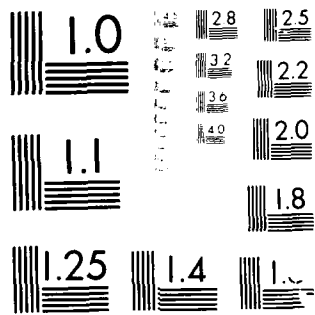
UNCLASSIFIED

TR-8806A(2948-06)-5 SD-TR-88-15

F/G 4/1

NL

END
DATE
FILMED
5 88



MICROCOPY RESOLUTION TEST CHART
 NATIONAL BUREAU OF STANDARDS-1963-A

AD-A191 164

Coordinated Ground and Space Measurements of an Auroral Surge over South Pole

T. J. ROSENBERG and D. L. DETRICK
Institute for Physical Science and Technology
University of Maryland
College Park, MD 20742

P. F. MIZERA and D. J. GORNEY
Space Sciences Laboratory
Laboratory Operations
The Aerospace Corporation
El Segundo, CA 90245

F. T. BERKEY
Center for Atmospheric and Space Physics
Utah State University
Logan, UT 84321

R. H. EATHER
Department of Physics
Boston College
Chestnut Hill, MA 02167

L. J. LANZEROTTI
AT&T Bell Laboratories
Murray Hill, NJ 07974

1 February 1988

Prepared for
SPACE DIVISION
AIR FORCE SYSTEMS COMMAND
Los Angeles Air Force Base
P.O. Box 92960, Worldway Postal Center
Los Angeles, CA 90009-2960

APPROVED FOR PUBLIC RELEASE:
DISTRIBUTION UNLIMITED

DTIC
S ELECTED D
APR 05 1988
H


88 4 4 1 10

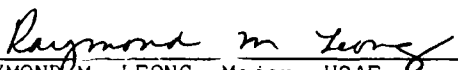
This report was submitted by The Aerospace Corporation, El Segundo, CA 90245, under Contract No. F04701-85-C-0086-P00016 with the Space Division, P.O. Box 92960, Worldway Postal Center, Los Angeles, CA 90009-2960. It was reviewed and approved for The Aerospace Corporation by H. R. Rugge, Director, Space Sciences Laboratory.

Lt Clarence V. Wilcox/CLTPC was the project officer for the Mission-Oriented Investigation and Experimentation (MOIE) Program.

This report has been reviewed by the Public Affairs Office (PAS) and is releasable to the National Technical Information Service (NTIS). At NTIS, it will be available to the general public, including foreign nationals.

This technical report has been reviewed and is approved for publication. Publication of this report does not constitute Air Force approval of the report's findings or conclusions. It is published only for the exchange and stimulation of ideas.


CLARENCE V. WILCOX, Lt, USAF
MOIE Project Officer
SD CLTPC


RAYMOND M. LEONG, Major, USAF
Deputy Director, AFSTC West Coast
Office
AFSTC/WCO OL-AB

REPORT DOCUMENTATION PAGE

1a REPORT SECURITY CLASSIFICATION Unclassified		1b. RESTRICTIVE MARKINGS	
2a SECURITY CLASSIFICATION AUTHORITY		3. DISTRIBUTION / AVAILABILITY OF REPORT Approved for public release; distribution unlimited.	
2b. DECLASSIFICATION / DOWNGRADING SCHEDULE		4. PERFORMING ORGANIZATION REPORT NUMBER(S) TR-0086A(2940-06)-5	
4. PERFORMING ORGANIZATION REPORT NUMBER(S) TR-0086A(2940-06)-5		5. MONITORING ORGANIZATION REPORT NUMBER(S) SD-TR-88-15	
6a. NAME OF PERFORMING ORGANIZATION The Aerospace Corporation Laboratory Operations	6b OFFICE SYMBOL (if applicable)	7a. NAME OF MONITORING ORGANIZATION Space Division	
6c. ADDRESS (City, State, and ZIP Code) El Segundo, CA 90245		7b ADDRESS (City, State, and ZIP Code) Los Angeles Air Force Station Los Angeles, CA 90009-2960	
8a. NAME OF FUNDING / SPONSORING ORGANIZATION	8b OFFICE SYMBOL (if applicable)	9 PROCUREMENT INSTRUMENT IDENTIFICATION NUMBER F04701-85-C-0086-P00016	
8c. ADDRESS (City, State, and ZIP Code)		10. SOURCE OF FUNDING NUMBERS	
		PROGRAM ELEMENT NO.	PROJECT NO.
		TASK NO.	WORK UNIT ACCESSION NO.
11 TITLE (Include Security Classification) Coordinated Ground and Space Measurements of an Auroral Surge over South Pole			
12. PERSONAL AUTHOR(S) Rosenberg, T. J., and Detrick, D. L., University of Maryland; Mizera, Paul F.,			
13a. TYPE OF REPORT	13b. TIME COVERED FROM _____ TO _____	14. DATE OF REPORT (Year, Month, Day) 1 February 1988	15 PAGE COUNT 34
16. SUPPLEMENTARY NOTATION			
17. COSATI CODES		18 SUBJECT TERMS (Continue on reverse if necessary and identify by block number)	
FIELD	GROUP	SUB-GROUP	
		Aurora Remote Sensing	
		Bremsstrahlung Riometer	
19 ABSTRACT (Continue on reverse if necessary and identify by block number) Coincident ground-based and satellite observations are presented of a premidnight auroral surge over Amundsen-Scott South Pole station. The set of near-simultaneous measurements provides an excellent opportunity to gain a more quantitative understanding of the nature of premidnight substorm activity at high geomagnetic latitudes. The surge produced a rapid onset of cosmic radio noise absorption at the station. On the polar-orbiting DMSP-F6 spacecraft, intense X-ray emissions with $E > 2$ keV energy were imaged 1 to 2 deg magnetically equatorward of the South Pole approximately 1 min prior to the peak of the absorption event. The precipitating electron spectrum determined from the X-ray measurements could be characterized by an e-folding energy of ~ 11 keV and is found to be adequate to account for the cosmic noise absorption and maximum auroral luminosity recorded at South Pole. Photometer, all-sky camera, riometer, and magnetometer data are used to estimate the velocity of motion and spatial extent of the auroral precipitation and the ionospheric currents associated with the surge. The electron precipitation region is deduced to have a latitudinal scale size of < 100 km and to have a poleward movement of $\sim 1-2$ km/s coincident with the			
20. DISTRIBUTION / AVAILABILITY OF ABSTRACT <input type="checkbox"/> UNCLASSIFIED/UNLIMITED <input checked="" type="checkbox"/> SAME AS RPT <input type="checkbox"/> DTIC USERS		21. ABSTRACT SECURITY CLASSIFICATION Unclassified	
22a. NAME OF RESPONSIBLE INDIVIDUAL		22b. TELEPHONE (Include Area Code)	22c. OFFICE SYMBOL

12. PERSONAL AUTHOR(S) (Continued)

and Gorney, David J., The Aerospace Corporation; Berkey, F. T., Utah State University; Eather, R. H., Boston College; and Lanzerotti, L. J., AT&T Bell Laboratories.

19. ABSTRACT (Continued)

movement of a westward electrojet. Northern auroral station magnetometer measurements also indicated the movement of a westward electrojet from local midnight toward the conjugate point of South Pole station at the same time. The photometric data are used to infer that precipitating electron fluxes ($E > 2$ keV) exceeded $200 \text{ ergs/cm}^2 \text{ s}$ and contributed to a vertical current density of $\sim 0.017 \text{ A/cm}$. This current density is comparable, to within a factor of ~ 2 , with the horizontal ionospheric current density ($\sim 0.028 \text{ A/cm}$) inferred from the ground-based magnetometer measurements at South Pole station. The presence of a large flux of electrons with $E < 2$ keV is discounted as an explanation for the difference on the basis that the expected 630 nm auroral luminosity would exceed by about an order of magnitude the luminosity that was observed ($< 1 \text{ kR}$).

CONTENTS

INTRODUCTION..... 7

MEASUREMENTS AND ANALYSIS..... 9

OBSERVATIONS..... 13

DISCUSSION..... 26

SUMMARY..... 32

REFERENCES..... 35



Prepared For	<input checked="" type="checkbox"/>
Checked by	
Reviewed by	
Approved by	
Signature	
Date	
Initials	
Remarks	
A-1	

FIGURES

1.	Spatial Distribution of $E > 2$ keV X-ray Energy Flux and Inferred Electron Energy Flux Observed by the Aerospace Scanning X-ray Spectrometer on DMSP-F6.....	14
2.	X-ray Differential Energy Spectra at 2358:04 UT on July 20, 1983, at the Point in the Scan of Figure 1 Where the Highest Intensity X-ray Fluxes Were Recorded.....	15
3.	Electron Precipitation Spectra Inferred from Ground-Based and Satellite Observations over the South Pole on July 20-21, 1983.....	18
4.	Ground-Based Data Acquired at South Pole Station Between 2200 UT on July 20 and 0200 UT on July 21, 1983.....	19
5.	South Pole Data, in the Interval from 2355 UT on July 20 to 0003 UT on July 21, Centered on the Event of Interest.....	21
6.	Sequence of All Sky Camera (ASC) Photographs Acquired at South Pole Station, Covering the Time Period Illustrated in Figure 5.....	23
7.	Scale Drawing of the Viewing Geometry of the Ground-Based and Satellite Instrumentation for the Coordinated DMSP-F6 and South Pole Station Observations.....	27

TABLES

1.	South Pole Instrumentation.....	10
2.	Broadbeam Riometer Absorption (A), Absorption Ratios (R), Inferred Zenithal Absorption (A_2), and Precipitation Width (W) at South Pole at 2359:14 UT.....	25
3.	Comparison of Electron Fluxes and Ionospheric Effects for Two Energy Spectrum Determinations.....	30

Introduction

Energetic electron precipitation as measured on the ground at high latitudes on the nightside is associated primarily with the westward traveling surge [Rostoker et al., 1980], a very dynamic event of small spatial scale initiated at the breakup of an auroral substorm [Meng et al., 1978; Inhester et al., 1981; Opgenoorth et al., 1983]. On occasion, however, high-latitude energetic electron precipitation has been reported by satellite measurements to occur in the form of isolated patches [e.g., Imhof et al., 1985]. A common manifestation in the nightside polar ionosphere of surge-type particle precipitation is a sharp spike in the absorption of cosmic radio noise [Nielsen and Axford, 1977; Hargreaves et al., 1979]. Absorption spikes are characterized by rapid onsets (≤ 1 min) and are produced by energetic electron precipitation ($E > 20$ keV) usually occurring within a narrow spatial region (≤ 50 km) located at the poleward border of a westward electrojet.

At auroral zone latitudes, absorption spikes are usually associated with the expansion phase of substorms [Nielsen and Greenwald, 1978; Nielsen, 1980; Nielsen et al., 1982], whereas Hones et al. [1986] have shown that at the geographic South Pole ($\lambda = 75^\circ$) such events typically occur in the late stage of magnetospheric substorms and appear to coincide closely in time with expansions of the plasma sheet at $\sim 18 R_E$ in the magnetotail.

During the first 8 months of 1983, approximately 100 rapid-onset absorption events, exceeding 0.5 dB at 30 MHz, were recorded at the Amundsen-Scott South Pole station in the 6-hr magnetic local time (MLT) interval 2100-0300 (at South Pole MLT = UT - 3.5 hrs). Southern hemisphere passes of the DMSP-F6

satellite occurred within a few minutes of the detected maximum absorption in 10 of these events. Of these, one event, which occurred at the end of July 20, 1983, when the Aerospace scanning X-ray spectrometer imaged the South Pole within 1 minute of the maximum measured absorption, provided a rare opportunity for comparisons of complementary measurements of electron precipitation, the visible aurora and ionospheric currents at South Pole.

A previous study using data from the P78-1 satellite and from the instruments at South Pole station [Imhof et al., 1984] found good agreement between the spatial and energy distributions of electron precipitation derived from satellite X-ray imaging ($E > 21$ keV) and the measured cosmic noise absorption. That study examined a short-lived (~ 10 s) precipitation spike associated with the apparent development of an eastward electrojet equatorward of the main precipitation region. The total rate of electron precipitation (deduced from the X-ray data) was approximately one-third that determined from the ionospheric current (i.e., magnetic field) variations. The discrepancy in that instance was attributed to underestimation of the incident electron fluxes with energies $\lesssim 20$ keV.

The present study differs from that of Imhof et al. [1984] in that 1) the July 20, 1983 event focuses on the onset-to-maximum absorption stage of the poleward leading edge of a precipitation region that produced a westward electrojet; 2) photometric and auroral imaging observations were available at South Pole station to better define the dynamical and morphological features of the event; and 3) the satellite X-ray data include the lower energy range ($E \lesssim 20$ keV) not previously available and more appropriate for comparison with the photometric and ionospheric current data. The morphological and spectral information provided by this set of ground and satellite measurements should aid in the evaluation of theoretical interpretations of surge events [e.g.,

Kan et al., 1984; Kan and Sun, 1985], particularly for those models in which the characteristic energy of the distribution of precipitating electrons influences the dynamics of the surge [Rothwell et al., 1984].

Measurements and Analysis

The plan of analysis was to determine the spectral characteristics and spatial distributions of the precipitating electrons using the DMSP-F6 satellite X-ray image in the vicinity of the South Pole. Unfortunately, DMSP optical imagery is not available for this time period. The satellite X-ray measurements and quantities derived therefrom were then compared to the intensity, spectral and spatial information inferred from riometer absorption, auroral luminosities, and ionospheric currents measured at South Pole station. The combined satellite and ground-based data sets provide more information on the morphology and dynamics of the precipitation event than can be acquired by any single observation alone.

A comprehensive set of ground-based instruments is available at South Pole station with which to study polar ionospheric phenomena. The particular measurements used in the present study were obtained by the sensor systems listed in Table 1. Data were sampled at 1 Hz and recorded on digital tape, except for the all-sky camera (ASC), which provided photographic images. Zenith-pointing photometers with a 55° field of view, approximately the same as that of the broadbeam riometer antennas, provided auroral luminosities at two wavelengths. Surface variations of the geomagnetic field were recorded in a left-hand coordinate frame with components in the north-south (H: positive north), east-west (D: positive east) and vertical (Z: positive upward) direction [Lanzerotti et al., 1982].

Table 1. South Pole Instrumentation

<u>Sensor</u>	<u>Institution</u>
All Sky Camera (ASC)	Utah State University
2-Channel Photometer (427.8 nm; 630.0 nm)	Boston College
Riometers (20.5; 30.0; 51.4 MHz)	University of Maryland
Fluxgate Magnetometer (H; D; Z)	AT&T Bell Laboratories

Auroral X-ray images were acquired with the Aerospace scanning X-ray spectrometer [Mizera et al., 1984, 1985a] on the DMSP-F6 satellite, which was in a sun-synchronous circular polar orbit at ~ 830 km altitude. The proportional counter (PC) X-ray spectrometer acquires a complete X-ray spectrum (2-70 keV in 24 differential channels) once per second while scanning from limb to limb across its ground track once every 20 seconds. A second set of X-ray sensors was also flown on the DMSP-F6 satellite. Three cadmium telluride (CdTe) solid-state detectors with integral thresholds above 15, 30 and 60 keV were mounted on a scanning head with the motion opposite to that of the PC scanning head [Mizera et al., 1985a]. The CdTe angular field of view in the cross track direction was approximately one-half that of the PC.

A raster image of X-ray intensity can be constructed from the combination of satellite motion and instrument scans. Furthermore, X-ray spectral information for $E > 2$ keV is available from the PC for each pixel in the image. Basic characteristics of the incident electron spectrum can be inferred from the bremsstrahlung X-ray spectra [e.g., Mizera et al., 1978; Miller and Vondrak, 1985; Imhof et al., 1985]. In this report, a least-squares technique is used to determine the electron spectral shape which most closely reproduces the observed X-ray spectrum.

Since the DMSP satellites are sun-synchronous, their orbital inclinations are such that the spacecraft never pass closer than 9° in latitude (~ 1000 km) to the poles. Thus, in situ electron measurements from the satellite cannot be used in this study, and remote sensing is required to obtain the precipitation pattern and spectra over the South Pole.

Observations

Figure 1 shows a portion of the southern hemisphere imaged by the Aerospace scanning X-ray spectrometer in the interval from 2353:24 UT on July 20 to 0002:24 UT on July 21, 1983. Dusk is at the bottom and dawn is at the top; midnight is to the left. The grid used in the images is geographic; 10° latitude (South) and 30° longitude (East) intervals are indicated. The symbol (+) identifies the location of the south geomagnetic pole.

The left panel in Figure 1 depicts the observed spatial distribution of integral X-ray energy fluxes for $E > 2$ keV. The precipitating electron energy fluxes inferred from the X-ray measurements are illustrated in the right panel. In both cases, the flux contours are logarithmic, with four contour levels per decade. The minimum X-ray flux contour plotted is 2×10^{-6} erg/cm² s; the minimum electron flux contour plotted is 1 erg/cm² s. Figure 1 shows that the highest intensity of bremsstrahlung X-rays and inferred electron energy fluxes occurred a few degrees away from the South Pole, toward midnight. At that point in the scan, the time was 2358:04 UT; the scan did not actually image the South Pole until 2358:24 UT. Note that the alignment of the flux contours at the magnetically poleward edge of the precipitation region is predominantly in the magnetic east-west direction, i.e., approximately perpendicular to a line from South Pole station to the geomagnetic pole.

Figure 2 (dashed curve) shows the X-ray differential number flux at energies of ~ 2 keV to 24 keV obtained from the proportional counter. These data were acquired at 2358:04 UT in the pixel that contained the maximum X-ray intensity. The vertical bars indicate the statistical counting errors. Above $E = 18$ keV, the spectrum flattens considerably, denoting a hardening of the X-ray fluxes at higher energies. Because the counting statistics from the

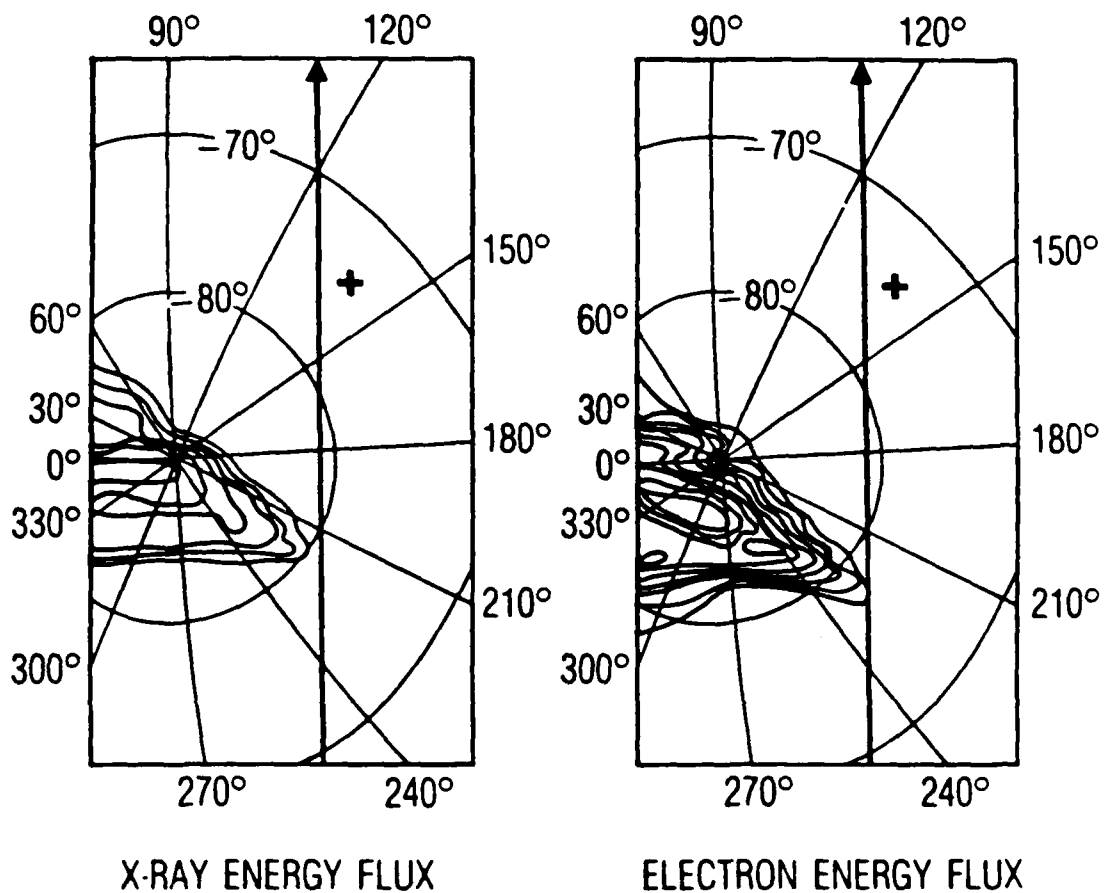


Figure 1. Spatial Distribution of $E > 2$ keV X-ray Energy flux (left) and Inferred Electron Energy Flux (right) Observed by the Aerospace Scanning X-ray Spectrometer on DMSP-F6. The image was acquired between 2353:24 UT on July 20 and 0002:24 UT on July 21, 1983, as the satellite traveled along the ground track marked with a heavy arrow. The contours are logarithmic, with four contour levels per decade. The minimum X-ray flux plotted is 2×10^{-6} erg/cm² s, and the minimum electron flux plotted is 1 erg/cm² s. Geographic coordinates are shown. Dusk is at the bottom, and dawn is at the top; midnight is to the left. The South magnetic pole is indicated by the (+) symbol.

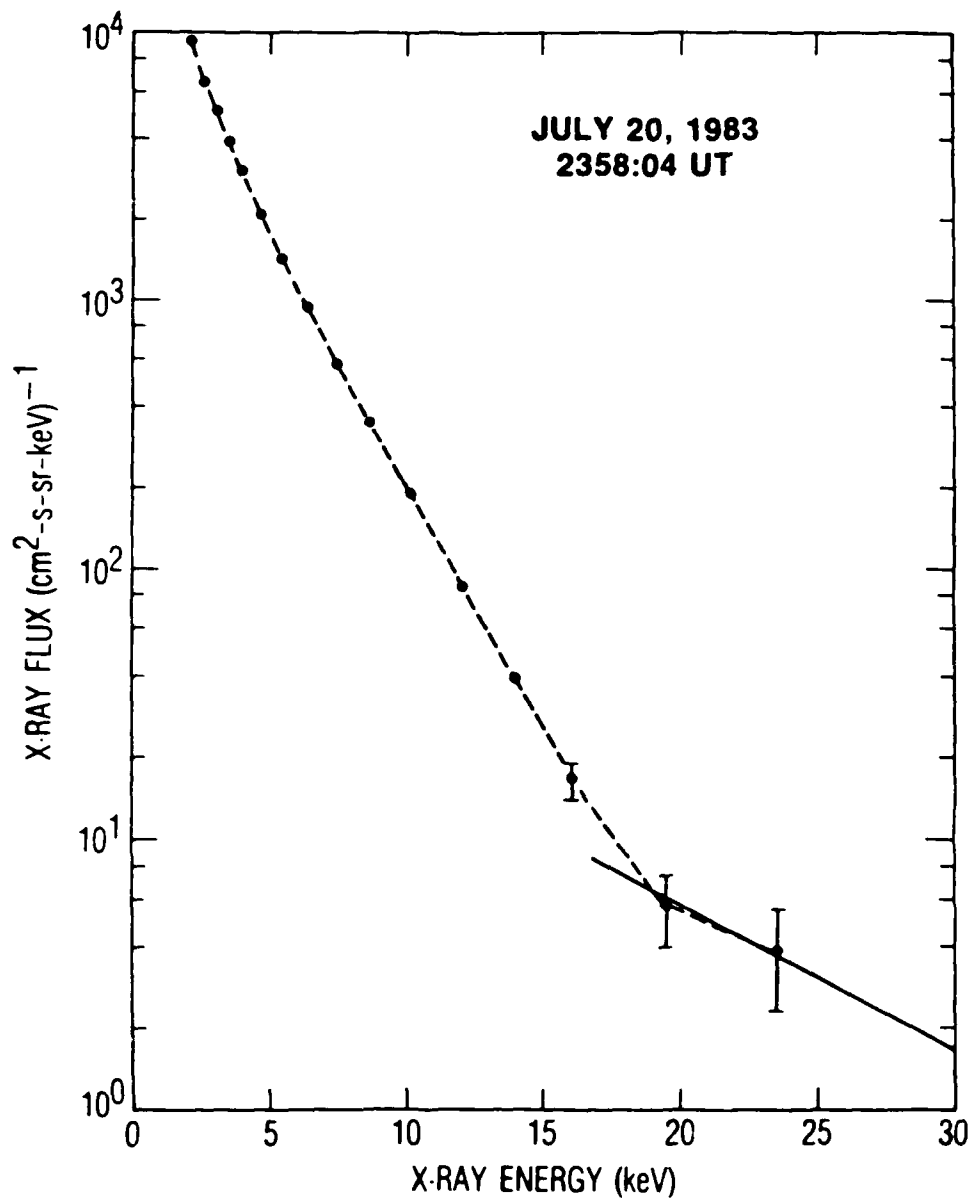


Figure 2. X-ray Differential Energy Spectra at 2358:04 UT on July 20, 1983, at the Point in the Scan of Figure 1 Where the Highest Intensity X-ray Fluxes Were Recorded. Counting rate uncertainties in the upper energy channels of the proportional counter are shown. The solid line is the X-ray spectrum derived from the cadmium telluride detectors.

proportional counter permitted only two points of the spectrum to be determined above 18 keV, the cadmium telluride detectors were used to 1) corroborate the apparent hardening of the X-ray spectrum above $E = 20$ keV and 2) examine with finer spatial resolution where the energetic electrons were precipitating. The solid line in Figure 2 was derived by differentiating the integral CdTe X-ray spectrum above $E = 15$ keV and normalizing it to the lower energy spectrum. All three CdTe sensors were used to sum the counts in each integral channel in order to decrease the statistical errors. The data show that the X-rays with $E \geq 15 - 20$ keV were co-located with the equatorial edge of the highest intensity contour of the X-ray energy fluxes in Figure 1 (left). The highest electron energy flux contour in Figure 1 (right) reflects the hardening of the X-ray spectrum at this location.

Two methods were used to derive the incident electron spectrum based on the X-ray differential spectrum shown in Figure 2. In the first method, a single exponential fit to the high-energy portion of the X-ray spectrum was used together with the results of Berger and Seltzer [1972] to infer an electron e-folding energy of 11 keV. This provided a convenient spectral parameter (i.e., the electron e-folding energy) for interpreting the results of the riometer measurements. As discussed below, the single component fit, employed in the energy range from 2 to 65 keV, could account satisfactorily for the observed luminosity and cosmic noise absorption.

In order to study the electron spectral shape in more detail, the electron spectrum was obtained from a least-squares analysis. In this method, a "first-guess" electron differential number flux spectrum is specified for energies comparable to those of the differential X-ray measurements. The bremsstrahlung X-ray spectrum which would result from the "first-guess" electron spectrum is

computed and compared to the observed X-ray spectrum. The electron flux spectrum is then varied iteratively until the sum of the normalized square deviations between the observed and computed X-ray spectra is minimized. A Levenberg-Marquardt numerical iteration scheme has been used, and consistent convergence has been experienced for a variety of initial spectral shapes when reasonable counting statistics are available.

The electron spectra derived by both methods are shown in Figure 3. The exponential characterization is in reasonable agreement with the approximate slope of the least-squares distribution. The irregular fluctuations at low energies (≤ 5 keV) of the least-squares spectrum are a manifestation of numerical difficulties in the bremsstrahlung deconvolution process at very low energies and should not be construed as real spectral features. For energies > 20 keV, the arrows indicate the maximum upper limits of the electron fluxes expected from the X-rays measured with the CdTe detectors. The derived electron spectrum reproduced the observed X-ray spectrum with a normalized chi-squared of 1.38. The optical emissions and cosmic radio noise absorption expected from electron fluxes with the spectra illustrated in Figure 3 are compared with the actual ground-based observations in a later section.

An overview of the responses of the 30 MHz riometer, the 427.8 nm photometer and the three-axis fluxgate magnetometer at South Pole for the 4 hrs centered on the event of interest is given in Figure 4. Auroral activity, as measured by the westward auroral electrojet index AL [WDC, 1986], is displayed in the bottom panel. The index was at quiet levels (~ 100 nT) until the onset of a magnetospheric substorm (arrow) at ~ 2330 UT on July 20, 1983. All sky images taken at South Pole between 2330 and 2355 UT (not shown) confirm that the very weak magnetic and photometric responses recorded at South Pole in that time interval were caused by electrojet currents and auroral intensifications

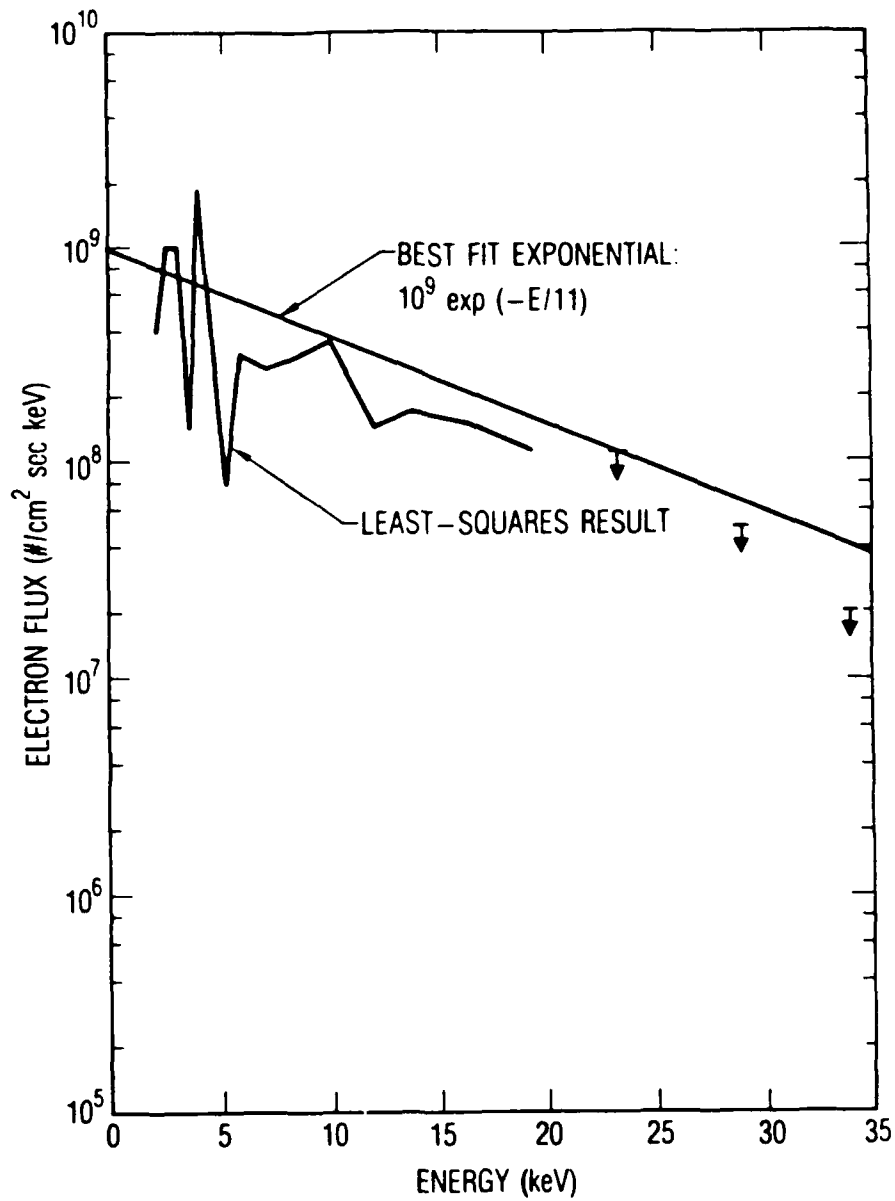


Figure 3. Electron Precipitation Spectra Inferred from Ground-Based and Satellite Observations over the South Pole on July 20-21, 1983. The solid line represents an exponential spectrum, which gives luminosity and absorption values consistent with the photometer and riometer observations. The spectrum inferred from satellite bremsstrahlung observations using the least-squares technique is indicated.

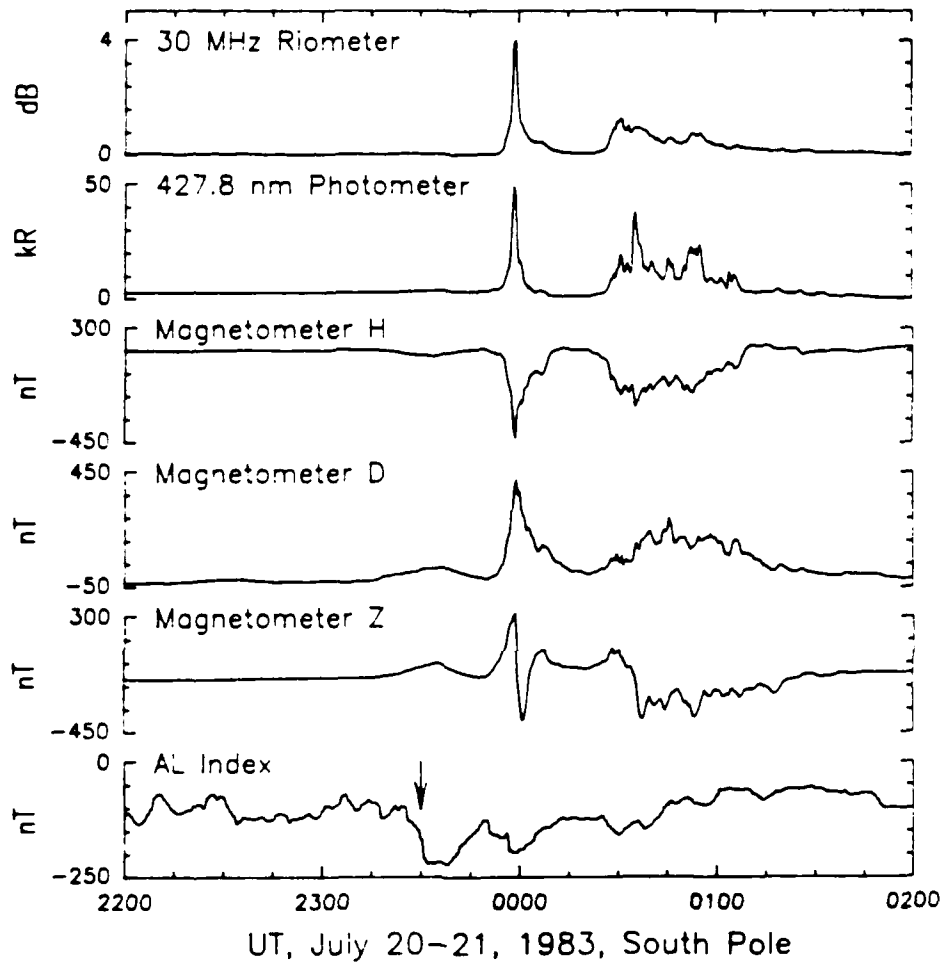


Figure 4. Ground-Based Data Acquired at South Pole Station Between 2200 UT on July 20 and 0200 UT on July 21, 1983. The plots include riometer absorption at 30 MHz, auroral luminosity at 427.9 nm, three components of magnetic variation, and the AL index. The onset of a magnetospheric substorm at approximately 2330 UT is indicated by the arrow. The surge event of interest occurred at ~ 0000 UT.

that were at or below $\Lambda = 70^\circ$.

The maximum negative horizontal magnetic component at the northern auroral stations that made up the AL index was recorded at Leirvogur, Iceland ($\Lambda = 66^\circ$), which was near local midnight. During the 2-min interval 2358 to 0000 UT, the maximum westward electrojet was recorded at Narssarssuaq, Greenland ($\Lambda = 68^\circ$), approximately 1 hour earlier in local time. Therefore, during the time period when South Pole station recorded the onset of the absorption event, the northern auroral stations indicated movement of the westward electrojet from midnight towards the dusk sector and closer to the magnetic conjugate location of the South Pole (approximately Frobisher Bay, Northwest Territories ($\Lambda = 74^\circ$)).

An expanded view of the South Pole data for the eight minutes centered on the interval of interest is shown in Figure 5. From ~ 2355 UT, rapid poleward motion of the auroral precipitation led to the increases in ionization, optical emission and magnetic variation that reached peak values near 2359 UT. The ionospheric current passed overhead at $\sim 2359:45$ UT when the Z-component magnetic variation crossed the baseline at -100 nT. The vertical dashed line at 2358:24 UT in Figure 5 marks the time when the satellite X-ray imager scanned the South Pole. This point in the scan occurred ~ 1 min before the particle precipitation and horizontal magnetic variation reached their maximum intensities and also ~ 1 min before the passage overhead of the local electrojet current. The observed surge of auroral activity occurred in the substorm recovery phase but was associated with an intensification of the westward electrojet in the auroral zone (see AL index in Figure 4). Recovery of the auroral and ionospheric disturbances in the vicinity of South Pole was largely complete by ~ 0010 UT on July 21. The subsequent, but less intense, activity that occurred between 0030 and 0100 UT (see Figure 4) is not examined in this

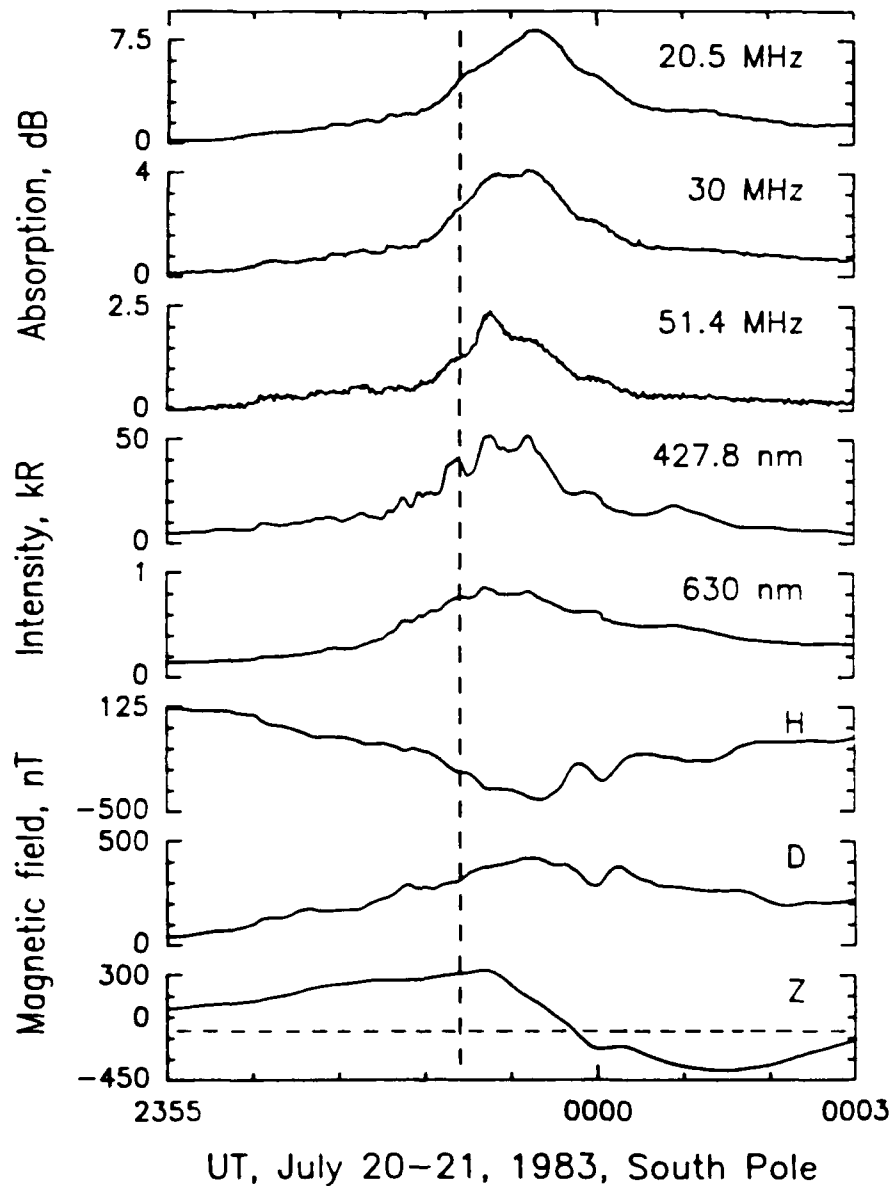


Figure 5. South Pole Data, in the Interval from 2355 UT on July 20 to 0003 UT on July 21, Centered on the Event of Interest. The vertical dashed line marks the time (2358:24 UT) when the satellite X-ray imager scanned the South Pole.

study.

The dynamics and morphology of the aurora in the vicinity of South Pole during this period are depicted in the sequence of all sky camera (ASC) images in Figure 6. Each image is a 16-sec exposure beginning on the minute. The orientation of the images in geomagnetic coordinates is given in the upper left image. Also indicated, by the concentric circle, is the portion of the ASC image at 100 km altitude that is viewed by the riometers and photometers. There is some obscuration by haze and by moonlight near the lower left of each image. The sequence of photos shows that auroral arcs, aligned mainly magnetic east-west, appeared on the equatorward horizon and moved rapidly poleward (at ~ 1 km/s estimated from the ASC data). This magnetic east-west alignment was also seen in Figure 1 in the alignment of the poleward edge of the electron energy contours derived from the X-ray flux contours imaged from space.

The most poleward arc in Figure 6 crossed the zenith during minute 2357. At this time, -1 dB absorption and ~ 10 kR luminosity were registered by the 30 MHz riometer and the 427.8 nm photometer, respectively. The magnetic variations indicate that the main precipitation and auroral current system were located equatorward (magnetically) of South Pole. During minute 2359 ± 1 min, the leading arc reached its most poleward extent ($\sim 56^\circ$ from the zenith), where it remained for the next several minutes. Aurora equatorward of this arc nearly filled the riometer and photometer fields of view during minute 2359 (during the largest magnetic excursion) and then decayed. By minute 0001 only the narrow poleward arc (≤ 25 km wide, as estimated from the ASC data) and a glow, principally due to moonlight near the equatorward edge, remained visible. The 427.8 nm photometer data in Figure 5 indicated several peaks between 2358:00 and 2359:30 UT, probably due to multiple arcs of energetic

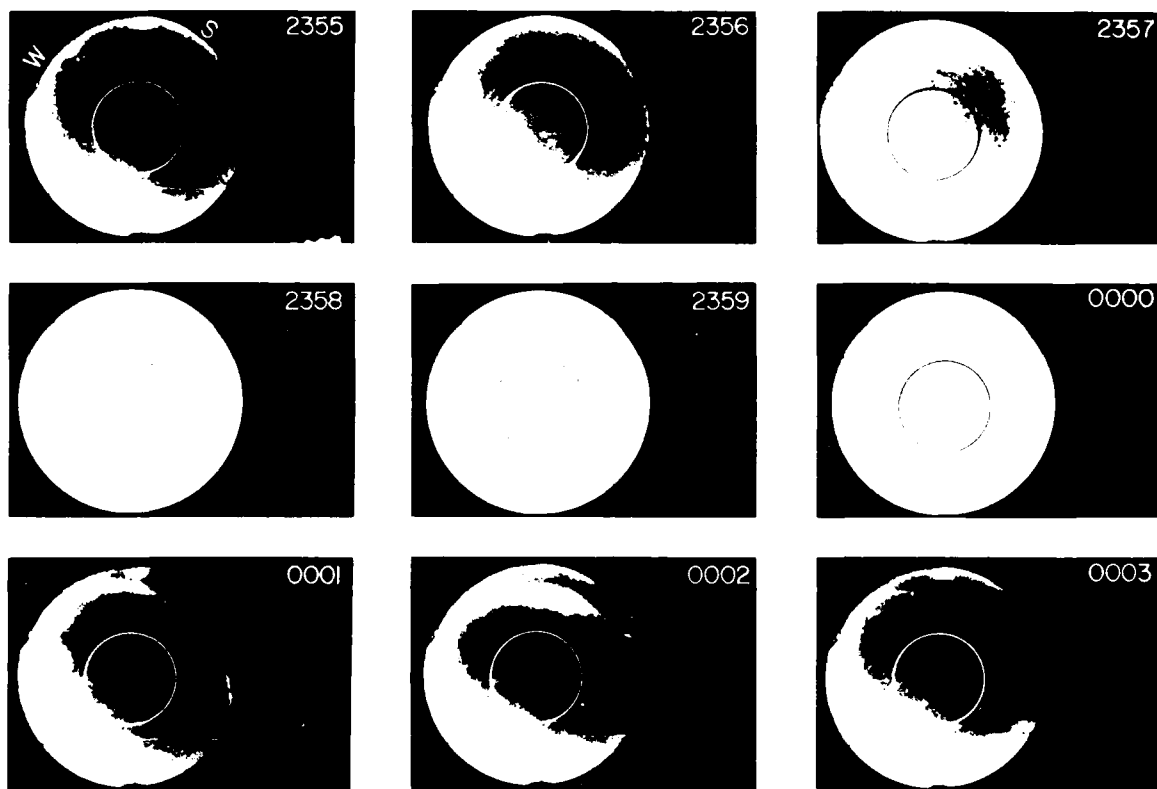


Figure 6. Sequence of All Sky Camera (ASC) Photographs Acquired at South Pole Station, Covering the Time Period Illustrated in Figure 5. Each image is a 16-sec exposure beginning on the minute. The orientation in magnetic coordinates is indicated on the top left image. Also indicated, by the concentric circle on each image, is that part of the image at 100 km altitude that is viewed by the riometers and photometer.

electron precipitation moving into the field of view and/or some enhancement in the precipitation rate. Some of this structure is also evident, but to a lesser extent, in the other ground-based data sets.

As previously mentioned, the main auroral current system passed overhead of South Pole at ~ 2359:45 UT. This occurred ~ 30 s after the peaks in the 20.5 MHz absorption, the 427.8 nm luminosity and the negative H-component magnetic bay and about 100 s after the maximum precipitation imaged by the satellite X-ray spectrometer 1°-2° magnetically equatorward of the South Pole; it is also consistent with the extent of the auroral disturbance as indicated by the ASC pictures. Assuming that the auroral current system can be represented as a horizontal thin line current at ~ 100 km altitude, aligned approximately perpendicular to the geomagnetic meridian through South Pole (as suggested by the ASC data), the change in the H-component of the magnetic field (~ 500 nT) implies a total current of ~ 2.5×10^5 A.

Table 2 gives the measured broadband absorptions (A_1 , A_2 and A_3) and absorption ratios for the three riometers (1, 2 and 3) at 20.5, 30, and 51.4 MHz frequencies at the time of the peak 30 MHz absorption (2359:14 UT). The peak absorption was essentially simultaneous at 20.5 and 30 MHz but occurred ~ 25 s earlier at 51.4 MHz. The measured absorption ratios ($R_{13} = 4.9$ and $R_{23} = 2.4$) are significantly lower than the values expected for an f^{-2} dependence (6.29 and 2.94, respectively). Based on the work of Hargreaves et al. [1979] and Imhof et al. [1984], one can infer from the observed ratios that the riometer beams are not uniformly filled by the electron precipitation regions. Employing the "Gaussian strip" model of Nielsen and Axford [1977] and Hargreaves et al. [1979], a precipitation region width $W \sim 89$ km at 2359:14 UT is obtained. This estimate of the width of the precipitation region is in reasonable quantitative agreement with the extended linear auroral forms observed in

Table 2. Broadbeam Riometer Absorption (A),
Absorption Ratios (R), Inferred Zenithal
Absorption (A_z) and Precipitation Width(W)
at South Pole at 2359:14 UT

A_1 (dB)	8.3
A_2 (dB)	4.1
A_3 (dB)	1.7
R_{13}	4.9
R_{23}	2.4
A_{z2} (dB)	6.9
A_{z3} (dB)	2.35 ± 0.45
W (km)	89 ± 24

1 = 20.5 MHz; 2 = 30.0 MHz; 3 = 51.4 MHz

the ASC photos. Table 2 also gives the equivalent zenithal 30 MHz and 51.4 MHz absorption values (A_z) which will be used for comparison with later calculations.

The peak intensity of the N_2^+ (427.8 nm) emission of 53 kR was reached at 2359:14 UT. At this time the oxygen red line intensity at 630 nm was < 1 kR, implying that the incident electron spectrum has a characteristic energy exceeding 10 keV [Rees and Luckey, 1974], consistent with the results of the X-ray analysis. The absolute intensity of the 427.8 nm emission can be used to estimate the total electron precipitation flux. Using $240 \text{ R/erg cm}^{-2} \text{ s}^{-1}$ for the conversion for spectra with characteristic energy above 10 keV [M. H. Rees, personal communication], the data in Figure 5 imply an energy deposition of approximately $220 \text{ ergs cm}^{-2} \text{ s}^{-1}$ during the peak absorption at 2359:14 UT.

Discussion

The viewing geometries of the ground-based riometer and photometer and the satellite-based X-ray imager are compared in Figure 7. The DMSP satellite is shown at its closest approach to South Pole. In this projection the satellite would be flying into the page. Various orientations of the X-ray imager field of view are shown in relation to the South Pole position and the nominal auroral altitude. The curvature of the Earth has been rectified in this drawing. The vertical cone at the South Pole represents the beam width of the riometers and the fields of view of the ground-based photometers. The projection of the intersection of this cone onto a horizontal surface at 100 km altitude is shown by the solid circle in the upper left of the figure. Note that the projection of the X-ray imager field of view in this orientation covers a larger area than the South Pole riometer cone at ~ 100 km altitude. In this projection, the field-of-view of the ASC (160° full angle) would correspond to a circle of

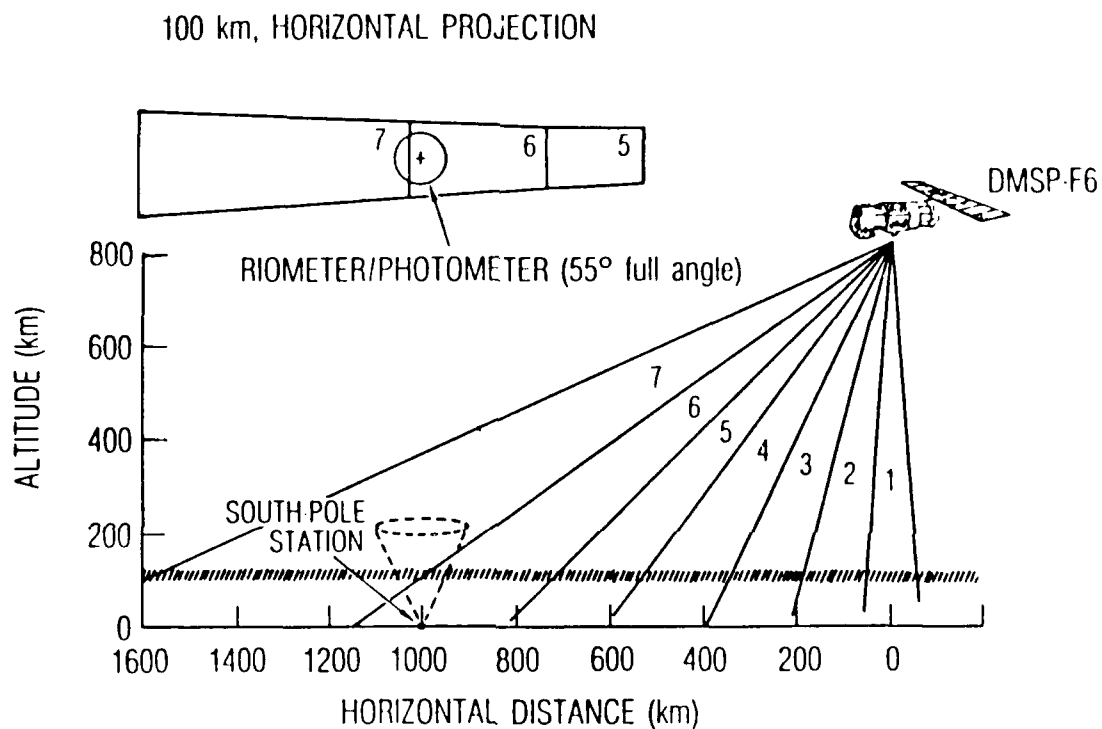


Figure 7. Scale Drawing of the Viewing Geometry of the Ground-Based and Satellite Instrumentation for the Coordinated DMSP-F6 and South Pole Station Observations. The numbers 1-7 indicate various viewing positions of the scanning X-ray spectrometer on DMSP. The field-of-view projections for the riometer and photometer on the 100 km horizontal surface are shown in the upper left portion of the figure.

radius - 600 km.

The geometric considerations of Figure 7 are important for interpreting the spatial distributions of X-ray and electron flux shown in Figure 1. The region of maximum electron precipitation in the satellite image occurs magnetically equatorward of the South Pole at 2358:04 UT and outside the effective viewing area of the zenith-centered photometers and riometers (a circle of - 52 km radius at - 100 km altitude). It is hypothesized that this region of maximum electron precipitation, observed by the X-ray imager approximately 1-2 degrees of latitude from the South Pole (- 150 km), moves toward the South Pole and is responsible for the peak absorption observed at the station 70 s later at 2359:14 UT. This hypothesis is consistent with the high poleward propagation speed (≥ 1 km/s) of the auroral arcs of Figure 6. Furthermore, as discussed below, the spectral characteristics of the precipitating electrons as inferred from riometry, photometry and X-ray spectrometry indicate a strong similarity between the intensity and spectral hardness of the precipitation region observed by the various techniques.

The differential electron number fluxes for an exponential spectrum with e-folding energy of 11 keV and as derived from the proportional counter X-ray data of Figure 2 using the least-squares analysis were presented in Figure 3. The derived spectrum represents the most intense bremsstrahlung activity (2358:04 UT), when the satellite was observing a region 1-2 degrees from South Pole station, toward the midnight sector. The ground-based instrumentation at the station recorded peak activity at 2359:14 UT. At this time the optical emission at 427.8 nm exceeded 50 kR, and the riometer data indicated that the zenithal absorption at 30 MHz was about 6.9 dB. For the purpose of comparison, we assume that the region of most intense precipitation moved overhead of South Pole station during the - 90-s interval between the satellite scan and

the observation of peak ground-based activity, and that the characteristics of the incident electron flux remained unchanged during this interval.

Table 3 summarizes the integral electron number and energy fluxes, the auroral luminosity and 30 MHz riometer absorption calculated from the electron spectrum derived by the least-squares technique and from the single 11 keV exponential spectrum. The calculations were performed for several electron energy ranges; the least-squares spectrum was extrapolated for energies greater than 35 keV. The observed 427.8 nm emission of ~ 50 kR and the zenithal 30 MHz riometer absorption of ~ 7 dB can be accounted for by the 11 keV exponential spectrum if the electron energy limit is extended to about 65 keV.

The electron fluxes derived by the least-squares technique appear insufficient to produce the observed light and cosmic noise absorption. However, these fluxes represent an average over the pixel scanning the precipitation region. From the width of the precipitation region (~ 90 km) estimated from the ground measurements, we calculate that only ~ 54% of the area of an X-ray pixel viewing the South Pole would be filled. Values of the electron flux, luminosity and absorption modified by this factor are in better agreement with those obtained from the exponential spectrum. This modified spectrum could be represented in Figure 3 by raising the least-squares curve by approximately a factor of 2.

Finally, it is of interest to compare the incident electron fluxes with the magnetometer estimate of the total horizontal ionospheric current of 2.5×10^5 A. Dividing this horizontal current by the 90 km width gives a horizontal current density of ~ 0.028 A/cm. For the 11 keV exponential spectrum, the total electron number flux of $1.1 \times 10^{10} \text{ cm}^{-2} \text{ s}^{-1}$ integrated over the 90 km width of the precipitation region represents a vertical current

Table 3. Comparison of Electron Fluxes
and Ionospheric Effects for Two Energy Spectrum Determinations

Exponential spectrum $f = 1.1 \times 10^9 \exp(-E/11)$	Energy range (keV)		
	$2 < E < 30$	$2 < E < 50$	$2 < E < 100$
Total current (electrons/cm ² -s)	9.3×10^9	1.1×10^{10}	1.1×10^{10}
Energy flux (ergs/cm ² -s)	158	200	212
Zenithal absorption (dB, 30 MHz)	3	5.5	8
Auroral Luminosity (kR, 427.8 nm)	38	48	51
<u>Least squares</u>			
Total current (electrons/cm ² -s)	5.8×10^9	6×10^9	6×10^9
Energy flux (ergs/cm ² -s)	98	110	110
Zenithal absorption (dB, 30 MHz)	2.4	3.4	3.7
Auroral Luminosity (kR, 427.8 nm)	24	26	26

density of ~ 0.016 A/cm. The corresponding value obtained from the modified least-squares spectrum is ~ 0.019 A/cm.

The ground-based and satellite-based inferences of precipitating electron flux and vertical current density are comparable to within a factor of two. Both underestimate somewhat the vertical current density required to balance the effective horizontal current density. Although lower energy electrons ($E < 2$ keV) could contribute significantly to the vertical current without producing much additional 427.8 nm luminosity or riometer absorption, the discrepancy in this instance cannot be explained this way. The presence of a large, additional low energy electron population is ruled out by the 630 nm optical data. A flux of $\sim 10^{10}$ $\text{cm}^{-2}\text{s}^{-1}$ below 2 keV would be required to balance the estimates of vertical and horizontal currents. Auroral electrons at these low energies can be characterized by a Maxwellian spectrum with energy parameter $\alpha = 0.6$ keV [M. H. Rees, personal communication]. From Rees and Luckey [1974], one then obtains a 427.8 nm intensity of 3 kR and a 630 nm/427.8 nm ratio of 3. Thus, a 630 nm intensity of 9 kR would be expected, whereas an order of magnitude less was observed (see Figure 5).

Uncertainty in the estimate of the precipitation region width also has a bearing on the quality of the comparison of vertical and horizontal currents. The agreement obtained in this event is better than was obtained, for example, in the work of Imhof et al. [1984].

Many of the morphological, dynamical and spectral features of the observed event are comparable to those previously observed in association with the westward traveling surge. Inhester et al. [1981] reported current densities of $1\text{--}10$ $\mu\text{A}/\text{m}^2$ over a 100×100 km patch, giving a total field-aligned current of $\sim 10^5$ A, comparable to the 2.5×10^5 A reported here. The field-aligned currents in a surge have been observed to be confined to the leading edge of

the pattern [Meng, 1978; Opgenoorth et al., 1983; Kan and Kamide, 1985], and electron precipitation at high energies (~ 10 keV) is common [e.g., Meng et al., 1978; Mizera and Gorney, 1981]. Velocities of surges are typically 1 to 2 km/s [Pytte et al., 1976], although higher instantaneous velocities have been reported [e.g., Opgenoorth et al., 1983; Yahnin et al., 1983].

In addition to the precipitation patterns, the current system morphology inferred from the northern auroral magnetometers (discussed in the previous section) implies that the westward electrojet moved from lower latitudes (Leirvogur and Narssarsuaq) with peak horizontal magnetic deflections of about -200 nT to the higher latitudes, with a maximum ΔH deflection of about 300 nT at South Pole station. South Pole station's magnetic conjugate point is near Frobisher Bay, which is 6 to 8 degrees higher in latitude and is located west of Leirvogur and Narssarsuaq. The maximum one-minute horizontal magnetic value changed from Leirvogur at 2358 to Narssarsuaq at 2359 UT on July 20, 1983. Note that the maximum South Pole station horizontal deflection occurred during minute 2359. Thus, the northern hemisphere magnetometer stations support the identification of the rapid-onset radio absorption event observed at South Pole on July 20, 1983, with an auroral surge propagating westward and poleward in both hemispheres. Evidence that westward traveling surges are conjugate was presented by Mizera et al. [1985b].

Summary

An auroral surge that produced a rapid-onset cosmic noise absorption event at South Pole station, Antarctica, has been studied with near-simultaneous ground-based and satellite observations. An X-ray image of the surge, when the region of maximum electron precipitation was located about one degree from the South Pole, was obtained by the DMSP-F6 satellite approximately one minute

prior to the peak of the absorption event. All sky camera images of the aurora obtained at South Pole indicated that the precipitation region moved from local midnight in the general direction of the magnetic pole at the rate of ~ 1 km/s. Complementary northern hemisphere auroral magnetograms suggest that a strong westward electrojet moved from local midnight toward the magnetic conjugate point of South Pole at this time. The latitudinal scale size of the region of maximum precipitation was determined from multi-frequency riometer measurements to be ~ 90 km and is consistent with the extent of auroral forms observable in the all-sky images.

The spectral form of the electron distribution at the time of maximum precipitation above South Pole could be characterized as exponential with a folding energy of ~ 11 keV and total energy flux ($E > 2$ keV) of ~ 200 ergs $\text{cm}^2\text{-s}$. This spectrum was sufficient to account for the maximum auroral luminosity at 427.8 nm and cosmic noise absorption recorded at South Pole. The inferred total energy flux is also consistent with the electron flux precipitating into the region of maximum X-ray intensity as imaged from space if the fraction of the image pixel filled by the precipitation is taken into account.

The electron flux ($E > 2$ keV) contributes a vertical current density of 0.016-0.19 A/cm over the ~ 90 -km width of the precipitation region, comparable to within a factor of 2 with the horizontal current density of 0.028 A/cm estimated from magnetometer measurements. The discrepancy in this instance cannot be accounted for by hypothesizing a large additional low energy electron population ($E < 2$ keV), as this is specifically ruled out by the low observed auroral luminosity at 630 nm.

References

- Hargreaves, J. K., H. J. A. Chivers, and E. Nielsen, Properties of spike events in auroral radio absorption, J. Geophys. Res., 84, 4245, 1979.
- Hones, E. W., Jr., T. J. Rosenberg, and H. J. Singer, Observed associations of substorm signatures at South Pole, at the auroral zone, and in the magnetotail, J. Geophys. Res., 91, 3314, 1986.
- Inhester, B., W. Baumjohann, R. A. Greenwald, and E. Nielsen, Joint two-dimensional observations of ground magnetic and ionospheric electric fields associated with auroral zone currents, 3: Auroral zone currents during the passage of a westward traveling surge, J. Geophys. 49, 155, 1981.
- Imhof, W. L., T. J. Rosenberg, L. J. Lanzerotti, J. B. Reagan, H. D. Voss, D. W. Datlowe, J. R. Kilner, E. E. Gaines, J. Mobilia, and R. G. Joiner, A coordinated satellite and ground-based study of an intense electron precipitation spike over the southern polar cap, J. Geophys. Res., 89, 10837, 1984.
- Imhof, W. L., H. D. Voss, D. W. Datlowe, and J. Mobilia, Bremsstrahlung X-ray images of isolated electron patches at high latitudes, J. Geophys. Res., 90, 6515, 1985.
- Kan, J. R., and Y. Kamide, Electrodynamics of the westward traveling surge, J. Geophys. Res., 90, 7615, 1985.
- Kan, J. R., R. L. Williams, and S. -I. Akasofu, A mechanism for the westward travelling surge during substorms, J. Geophys. Res., 89, 2211, 1984.
- Kan, J. R., and W. Sun, Simulation of the westward traveling surge and P12 pulsations during substorms, J. Geophys. Res., 90, 10911, 1985.
- Lanzerotti, L. J., L. V. Medford, and T. J. Rosenberg, Magnetic field and particle precipitation observations at the South Pole, Antarc. J. of the U.S., 17, 235, 1982.

- Meng, C. -I., Electron precipitations and polar auroras, Space Sci. Rev., 22, 223, 1978.
- Meng, C. -I., A. L. Snyder, Jr., and H. W. Kroehl, Observations of auroral westward travelling surges and electron precipitations, J. Geophys. Res., 83, 575, 1978.
- Miller, K. L., and R. R. Vondrak, A high-latitude phenomenological model of auroral precipitation and ionospheric effects, Radio Science, 20, 431, 1985.
- Mizera, P. F., J. G. Luhmann, W. A. Kolasinski, and J. B. Blake, Correlated observations of auroral arcs, electrons and X-rays from a DMSP satellite, J. Geophys. Res., 83, 5573, 1978.
- Mizera, P. F., and D. J. Gorney, S3-3 studies of the surge aurora, EOS, 62, 1003, 1981.
- Mizera, P. F., D. J. Gorney, and J. L. Roeder, Auroral X-ray images from DMSP-F6, Geophys. Res. Lett., 83, 255, 1984.
- Mizera, P. F., W. A. Kolasinski, D. J. Gorney, and J. L. Roeder, An auroral X-ray imaging spectrometer, J. Spacecraft and Rockets, 22, 514, 1985a.
- Mizera, P. F., D. J. Gorney, and H. Kroehl, Auroral precipitation and ionospheric currents, EOS, 66, 1005, 1985b.
- Moshupi, M. C., C. D. Anger, J. S. Murphree, D. D. Wallis, J. H. Whitteker, and L. H. Brace, Characteristics of trough region auroral patches and detached arcs observed by ISIS2, J. Geophys. Res., 84, 1333, 1979.
- Nielsen, E., Dynamics and spatial scales of auroral absorption spikes associated with the substorm expansion phase, J. Geophys. Res., 85, 2092, 1980.
- Nielsen, E., and W. I. Axford, Small scale auroral absorption events associated with substorms, Nature, 267, 502, 1977.

- Nielsen, E., and R. A. Greenwald, Variations in ionospheric currents and electric fields in association with absorption spikes during the substorm expansion phase, J. Geophys. Res., 83, 5645, 1978.
- Nielsen, E., A. Korth, G. Kremser, and F. Mariani, The electron pitch angle distribution at geosynchronous orbit associated with absorption spikes during the substorm expansion phase, J. Geophys. Res., 87, 887, 1982.
- Opgenoorth, H. J., R. J. Pellinen, W. Baumjohann, E. Nielsen, G. Marklund, and L. Eliasson, Three dimensional current flow and particle precipitation in a westward traveling surge observed during the Barium-GEOS rocket experiment, J. Geophys. Res., 88, 3138, 1983.
- Pytte, T., R. L. McPherron, and S. Kokubun, The ground signatures of the expansion phase during multiple onset substorms, Planet. Space Sci., 24, 1115, 1976.
- Rees, M. H., and D. Luckey, Auroral electron energy derived from the ratio of spectroscopic emissions, 1: Model computations, J. Geophys. Res., 79, 5181, 1974.
- Rostoker, G., S. -I. Akasofu, J. Foster, R. A. Greenwald, Y. Kamide, K. Kawasaki, A. T. Y. Lui, R. L. McPherron, and C. T. Russell, Magnetospheric substorms: Definitions and signatures, J. Geophys. Res., 85, 1663, 1980.
- Rothwell, P. L., M. B. Silevitch, and L. P. Block, A model for the propagation of the westward traveling surge, J. Geophys. Res., 89, 8941, 1984.
- World Data Center C2 for Geomagnetism, Auroral electrojet indices (AE) July - December 1983, Data Book No. 13, Kyoto University, Kyoto, Japan, 1986.
- Yahnin, A. G., V. A. Sergeev, R. J. Pellinen, W. Baumjohann, K. A. Kaila, H. Ranta, J. Kangas, and O. M. Raspopov, Substorm time sequence and microstructure on 11 November 1976, J. Geophys., 53, 182, 1983.

LABORATORY OPERATIONS

The Aerospace Corporation functions as an "architect-engineer" for national security projects, specializing in advanced military space systems. Providing research support, the corporation's Laboratory Operations conducts experimental and theoretical investigations that focus on the application of scientific and technical advances to such systems. Vital to the success of these investigations is the technical staff's wide-ranging expertise and its ability to stay current with new developments. This expertise is enhanced by a research program aimed at dealing with the many problems associated with rapidly evolving space systems. Contributing their capabilities to the research effort are these individual laboratories:

Aerophysics Laboratory: Launch vehicle and reentry fluid mechanics, heat transfer and flight dynamics; chemical and electric propulsion, propellant chemistry, chemical dynamics, environmental chemistry, trace detection; spacecraft structural mechanics, contamination, thermal and structural control; high temperature thermomechanics, gas kinetics and radiation; cw and pulsed chemical and excimer laser development including chemical kinetics, spectroscopy, optical resonators, beam control, atmospheric propagation, laser effects and countermeasures.

Chemistry and Physics Laboratory: Atmospheric chemical reactions, atmospheric optics, light scattering, state-specific chemical reactions and radiative signatures of missile plumes, sensor out-of-field-of-view rejection, applied laser spectroscopy, laser chemistry, laser optoelectronics, solar cell physics, battery electrochemistry, space vacuum and radiation effects on materials, lubrication and surface phenomena, thermionic emission, photo-sensitive materials and detectors, atomic frequency standards, and environmental chemistry.

Computer Science Laboratory: Program verification, program translation, performance-sensitive system design, distributed architectures for spaceborne computers, fault-tolerant computer systems, artificial intelligence, micro-electronics applications, communication protocols, and computer security.

Electronics Research Laboratory: Microelectronics, solid-state device physics, compound semiconductors, radiation hardening; electro-optics, quantum electronics, solid-state lasers, optical propagation and communications; microwave semiconductor devices, microwave/millimeter wave measurements, diagnostics and radiometry, microwave/millimeter wave thermionic devices; atomic time and frequency standards; antennas, rf systems, electromagnetic propagation phenomena, space communication systems.

Materials Sciences Laboratory: Development of new materials: metals, alloys, ceramics, polymers and their composites, and new forms of carbon; non-destructive evaluation, component failure analysis and reliability; fracture mechanics and stress corrosion; analysis and evaluation of materials at cryogenic and elevated temperatures as well as in space and enemy-induced environments.

Space Sciences Laboratory: Magnetospheric, auroral and cosmic ray physics, wave-particle interactions, magnetospheric plasma waves; atmospheric and ionospheric physics, density and composition of the upper atmosphere, remote sensing using atmospheric radiation; solar physics, infrared astronomy, infrared signature analysis; effects of solar activity, magnetic storms and nuclear explosions on the earth's atmosphere, ionosphere and magnetosphere; effects of electromagnetic and particulate radiations on space systems; space instrumentation.

...

FILMED
58